Experiments and simulations of Ar scattering from an ordered 1-decanethiol–Au(111) monolayer

K. D. Gibson, N. Isa, and S. J. Sibener[a]
The James Franck Institute and Department of Chemistry, The University of Chicago, Chicago, Illinois 60637

A study of the scattering of Ar from a well-ordered standing-up phase of 1-decanethiol adsorbed on Au(111) at surface temperatures from 110 to 185 K is presented. The final energies and intensities were measured as a function of incident polar and azimuthal angles using incident energies from 65 to 600 meV. These experimental results are compared to classical trajectory calculations. Scattering shows two distinct exit channels. The higher energies are due to direct inelastic scattering and have the greatest intensities at glancing incident and final angles. The lower energy channel is due to trapping-desorption; it has a Maxwell–Boltzmann energy distribution at the surface temperature and a cosine angular intensity profile. The simulations show that the timescale for normal momentum accommodation is very fast. The parallel momentum accommodation takes slightly longer, dependent on the initial conditions, but is still complete within only a few picoseconds. The result is that much of the Ar undergoes trapping-desorption, and the promptly scattered direct inelastic component, which interacts with the surface for ~1 picosecond, retains more of its parallel than perpendicular momentum, leaving the surface preferentially at glancing polar angles. Another interesting observation is that the energy exchange between the surface and the directly scattered Ar has a dependence on the incident azimuthal angle. This is, in a sense, another type of structure scattering, where it is the anisotropic elastic response of the surface rather than the corrugation that leads to the angular dependence of the atom scattering. © *2003 American Institute of Physics.*
[DOI: 10.1063/1.1628672]

INTRODUCTION

The interaction of gases with surfaces is of primary importance in understanding many fundamental processes including, for example, aerodynamic drag, the catalytic activity of transition metals, the erosion of polymers in low earth orbit, and the absorption of oxygen by the organic membranes lining our lungs. A first step in many of these processes involves dissipating some of the translational energy of the colliding gas atom or molecule. Frequently, complete translational energy accommodation with the surface is a necessary step in a surface mediated reaction.

The utilization of inert gases is a good starting point towards understanding translational energy transfer between a surface and an impinging gas molecule. They have simple, spherically symmetric interactions that can be reasonably well calculated, and have been experimentally measured in many instances. Further, measurements can be made without the complication of a time-varying surface due to chemical reaction products. Another advantage is that it is experimentally quite easy to make rare gas beams with different kinetic energies and relatively narrow energy dispersion.

The interaction of rare gases with metal surfaces has been extensively studied, both experimentally[1] and theoretically.[2,3] For the thermal energies used in this paper (<0.625 eV), there are two principal scattering channels, the

higher energy attributed to direct inelastic scattering and the lower energy attributed to trapping-desorption. The former generally leaves the surface with an intensity profile peaked super-specularly and with little change in parallel momentum. The trapping-desorption channel usually has a Maxwell–Boltzmann energy distribution appropriate to the surface temperature, T_s, and a cosine angular intensity profile,[4] though noncosine intensities and Maxwell–Boltzmann energy distributions with a characteristic temperature less than T_s have been seen for chemically modified surfaces.[5]

Although the majority of noble gas scattering has been done with solid surfaces, organic liquid surfaces have also been studied.[6] They generally exhibit the same two scattering channels. In this case, a good first approximation to the direct inelastic scattering channel is to treat the Ar as having scattered off protruding functional groups, considered to be spherical. Interestingly, the fraction of trapped and desorbed atoms increases with T_s, the opposite of the behavior on smooth metals.[1–3] This is attributed to a roughening of the surface, which fosters multiple collisions and a more complete accommodation of the incident momentum of the Ar. Recently, in an attempt to better understand atmospheric chemistry, Ar–ice collisions have been studied.[7] The Ar was seen to rapidly and efficiently exchange energy with ice, and at a 1.0 eV incident energy at $T_s = 180$ K as much as a third of the Ar actually penetrates below the surface. Lastly, the Morris group has experimentally examined rare gas col-

[a]Author to whom correspondence should be addressed. Electronic mail: s-sibener@uchicago.edu

TABLE I. Parameters for the Ar–CH$_4$ parameters.

Parameter	Value	Units
a	3.72×10^6	kcal/mole Å^{12}
b	-787.1	kcal/mole Å^6
c	3.381×10^5	kcal/mole
d	3.657	Å^{-1}
f	-1.282×10^5	kcal/mole Å^9

lisions with self-assembled monolayers (SAMs).[8] In contrast to the experiments described in this paper, their study was principally concerned with the effects of different terminal groups on the SAM overlayer.

Previously, our group has studied Ne scattering from an ordered, standing overlayer of 1-decanethiol adsorbed on Au(111),[9,10] which was partially motivated by previous theoretical results of the Hase group.[11–14] This surface is different from the metals because it is highly corrugated, has large thermal motion, and is relatively "soft." It varies from the liquids, at least in part, because it has good long-range order. Experimentally it was found that under most conditions that there are apparently two channels for the scattering. The direct inelastic dominates under most conditions, showing the least energy exchange and greatest intensity for grazing incident and exit angles. The slow channel has an energy much higher than a Maxwell–Boltzmann distribution at T_s, and does not have a cosine angular intensity profile. Neither par-
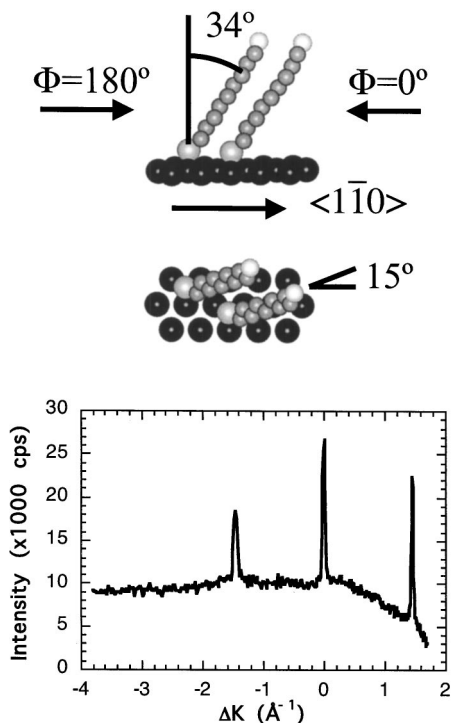

FIG. 1. Schematic of the 1-decanethiol–Au surface showing the chain tilt with respect to the Au surface plane and the rotation angle with respect to the $\langle 1\bar{1}0 \rangle$ direction. In this paper, the azimuthal angle of the incoming Ar (the angle in the surface plane) Φ_i, is defined as 180° for scattering along the $\langle 1\bar{1}0 \rangle$ direction (approximately with the chain tilt) and 0° in the opposite direction (approximately against the chain tilt). The bottom panel shows a He diffraction spectrum taken with $\Theta_F = 45°$ and $T_S = 135$ K.
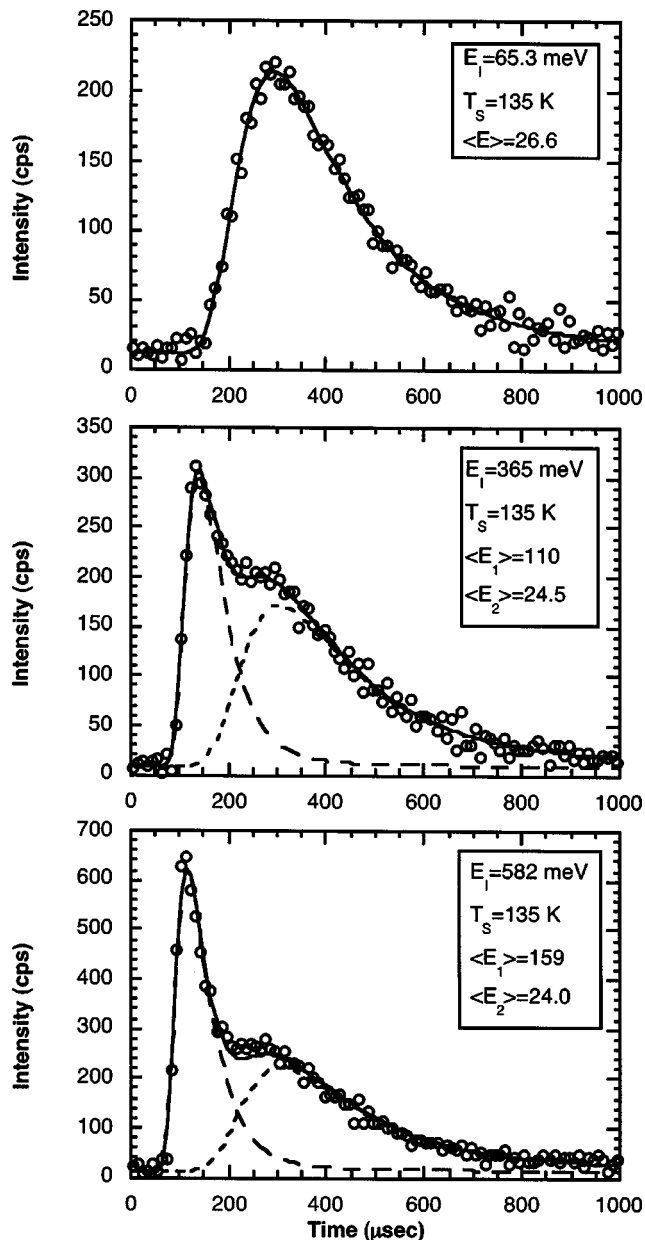

FIG. 2. Example TOF spectra with $\Theta_i = 45°$ and $\Theta_f = 50°$ at three different initial energies, $T_s = 135$ K and $\Phi_i = 0°$. Circles are the data, solid line is the total fit to the data, and the dashed lines are the individual contributions of each velocity distribution, where appropriate.

allel nor perpendicular momentum is conserved. From the classical simulations, it is apparent that the Ne does not exchange nearly as much of its initial momentum with the surface as do the heavier rare gases. In addition, a rather shallow potential well relative to the surface temperature means that much of the Ne scatters after only a short interaction time, leading to the intense direct inelastic channel. The relative slowness of the momentum accommodation with the surface relative to the residence time helps explain why the slow component is relatively warm with respect to a Maxwell–Boltzmann distribution at the surface temperature.

In this paper, we describe experiments where these studies are continued with Ar, which is both heavier and has a deeper potential well. Experimentally, this was done over a
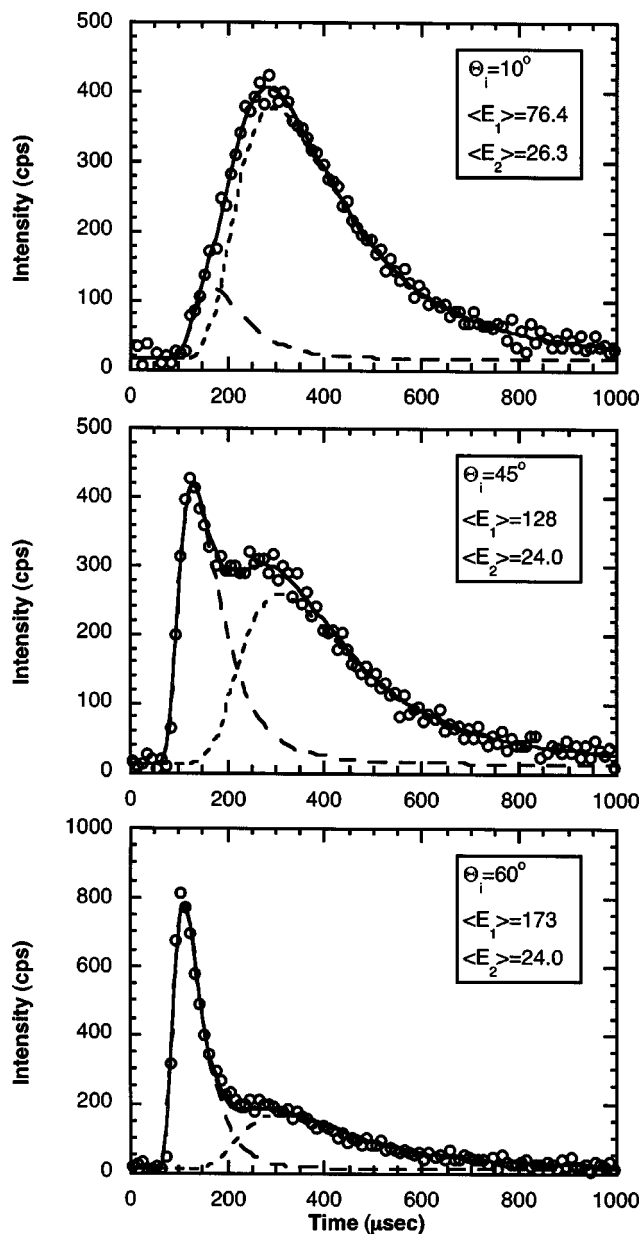
FIG. 3. Example TOF spectra with $\Theta_f = 40°$ and $E_i = 582$ meV at three different incident angles, $T_s = 135$ K and $\Phi_i = 0°$. Circles are the data, solid line is the total fit to the data, and the dashed lines are the individual contributions of each velocity distribution.

FIG. 4. Example TOF spectra with $\Theta_i = 30°$ and $E_i = 365$ meV at three different final angles, $T_s = 135$ K and $\Phi_i = 0°$. Circles are the data, solid lines are the total fit to the data, and the dashed lines are the individual contributions of each velocity distribution.

range of incident polar angles, Θ_i, from 10° to 60°, T_s from 110 to 185 K, incident energies, E_i from 65 to 600 meV, and different incident azimuths, Φ_i. In a following paper,[15] the scattering of Xe will be described, along with a comparison of the surface interactions for the three rare gases.

EXPERIMENT AND TRAJECTORY CALCULATIONS

The experimental apparatus and methods have been covered elsewhere,[9,16] so only a brief description will be presented. The experiments were carried out in an ultrahigh vacuum molecular beam scattering machine that contained an independently rotatable crystal manipulator and quadrupole mass spectrometer detector. The arc formed by the detector rotation defines the plane in which scattered atoms can
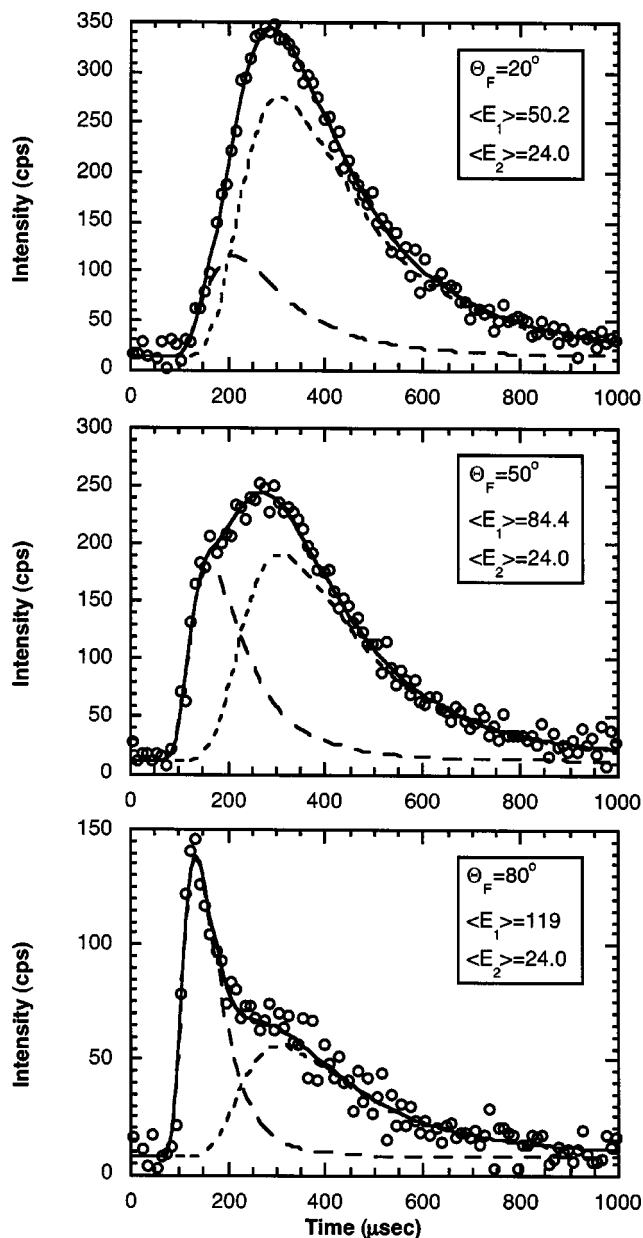
be detected. The Au(111) crystal could be resistively heated and cooled with liquid nitrogen. Cleanliness and order could be checked with Auger electron spectroscopy and He atom beam scattering. All of the data were taken using a post-collision mechanical cross-correlation chopper that was mounted on, and rotated with, the differentially pumped and collimated detector. Growth of the monolayer was done by exposing the 280 K Au crystal to a beam of He that had been bubbled through 1-decanethiol in a heated reservoir. Molecular beams of Ar were made by the supersonic expansion at room temperature of the following gas mixtures: Neat Ar [65.3 meV, full width at half maximum (FWHM)=17 meV], Ar–He (365 meV, FWHM=42 meV), and Ar–H$_2$ (582 meV, FWHM=50 and 625 meV, FWHM=52 meV).
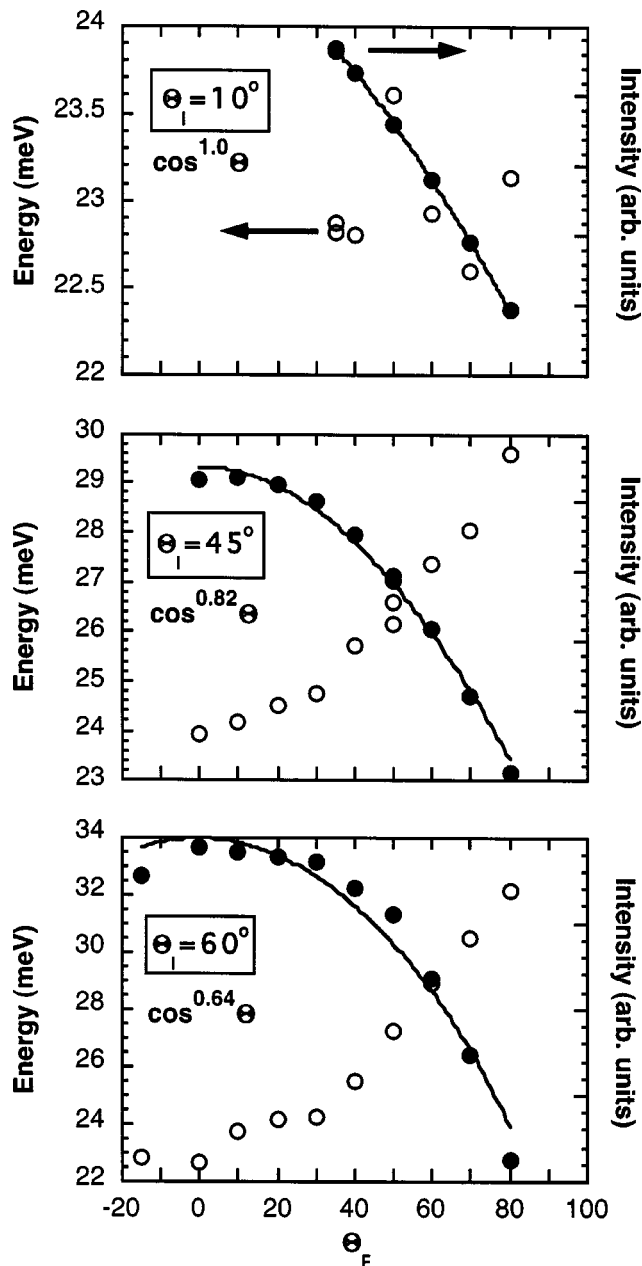
The scattering calculations were done with the VENUS

FIG. 5. Average energy (open circles) and intensity (filled circles) as a function of final angle for $E_i = 65.3$ meV for different incident angles, $T_s = 135$ K and $\Phi_i = 0°$. The solid lines are from fits to $\cos^n(\Theta_f)$.

FIG. 6. Average energy (open circles) and relative average intensities (filled symbols) as a function of final angle for $E_i = 365$ meV, $T_s = 135$ K and $\Phi_i = 0°$. For $\Theta_i \geqslant 30°$, the fit is comprised of a direct inelastic and a trapping-desorption component with the intensities represented by circles and squares respectively. The angular intensity distribution of the trapping-desorption is distributed as $\cos(\Theta_f)$ and the value of T in the Maxwell–Boltzmann distributions is 139 K for $\Theta_i = 30°$ and $60°$ and 142 K for $\Theta_i = 45°$.

code[17] using a 36 chain slab, with the addition of periodic boundary conditions to mimic a larger surface without the computational overhead.[18] As with the Ne simulations, a united atom model was used, where the hydrogens and carbon are rigidly connected. Only the Ar–CH$_3$ and –CH$_2$ potentials were used for the interaction, derived by fitting the results of Ar–CH$_4$ crossed-beam scattering experiments[19] to the equation

$$V(r) = a/r^{12} + b/r^6 + c \cdot \exp(-dr) + f/r^9. \tag{1}$$

The parameters are listed in Table I. These values give a highly corrugated surface. The corrugation of the static surface is as much as ~1 Å, and the well depth varies from 33
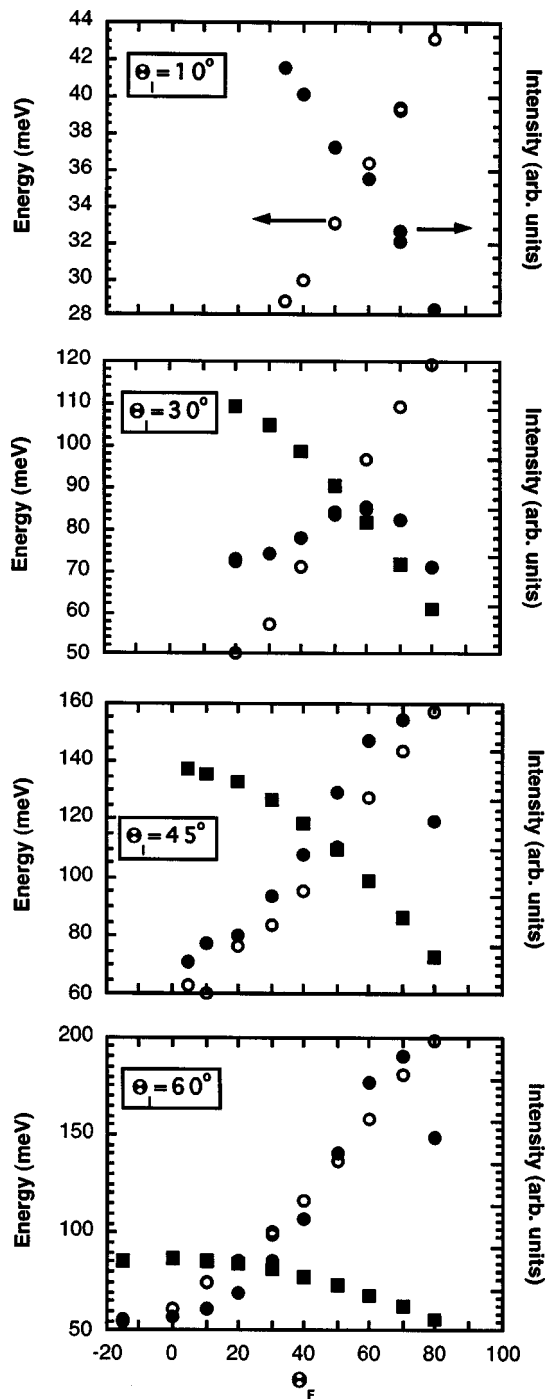
meV at a top site and 67 meV in the center of the rhombus formed by four surface methyl groups. The surface also has a large thermal excursion, with the root-mean-square movement of 0.28 Å in the surface normal direction at a surface temperature $T_s = 135$ K.

A schematic of the surface is shown in Fig. 1. The one angle not labeled is the twist angle Ψ, measured between the
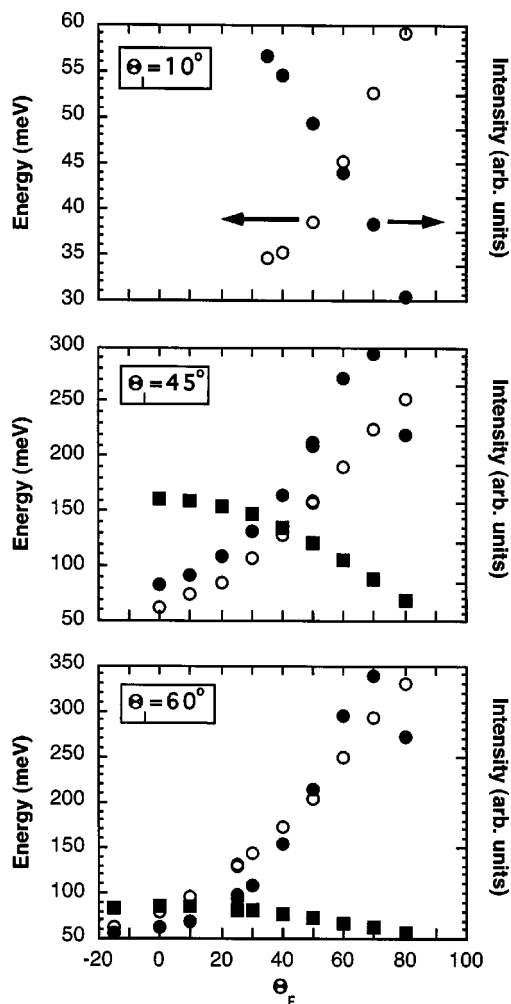
FIG. 7. Average energy (open circles) and relative average intensities (filled symbols) as a function of final angle for $E_i = 582$ meV, $T_s = 135$ K, and $\Phi_i = 0°$. For $\Theta_i \geqslant 45°$, the fit is comprised of a direct inelastic and a trapping-desorption component with the intensities represented by circles and squares respectively. The angular intensity distribution of the trapping-desorption is distributed as $\cos(\Theta_f)$ and the value of T in the Maxwell–Boltzmann distributions is 139 K.

FIG. 9. Experimental scattering probabilities (filled circles) compared with simulation results (open circles) plotted vs final energy, with $T_s = 135$ K and $\Phi_i = 0°$. The experimental distributions are the weighted sum of the results over the full range of Θ_f sampled. Simulation results use the trajectories that fall within this range of Θ_f. For $E_i = 65.3$ meV, the lines are from fits to a Maxwell–Boltzmann energy distribution with T given in the inset, and scattering at all azimuths is used for the simulation results. For higher incident energies, the range of azimuths used was $\pm 40°$ from the scattering plane. The bottom panel also includes some error bars for higher energies. Over the same energy range, the error bars from the fits of the summed data sets are only slightly larger than the size of the symbols. The solid line is from a fit to two Maxwell–Boltzmann distributions, one shifted and one at T_S, as in Eq. (2).
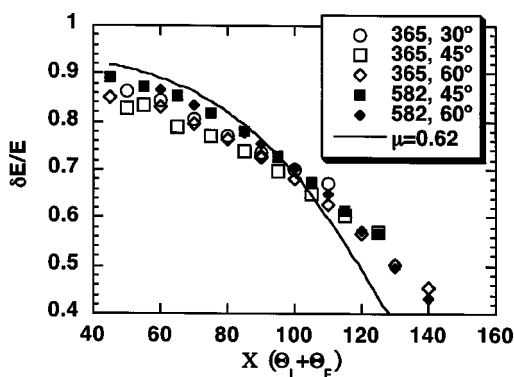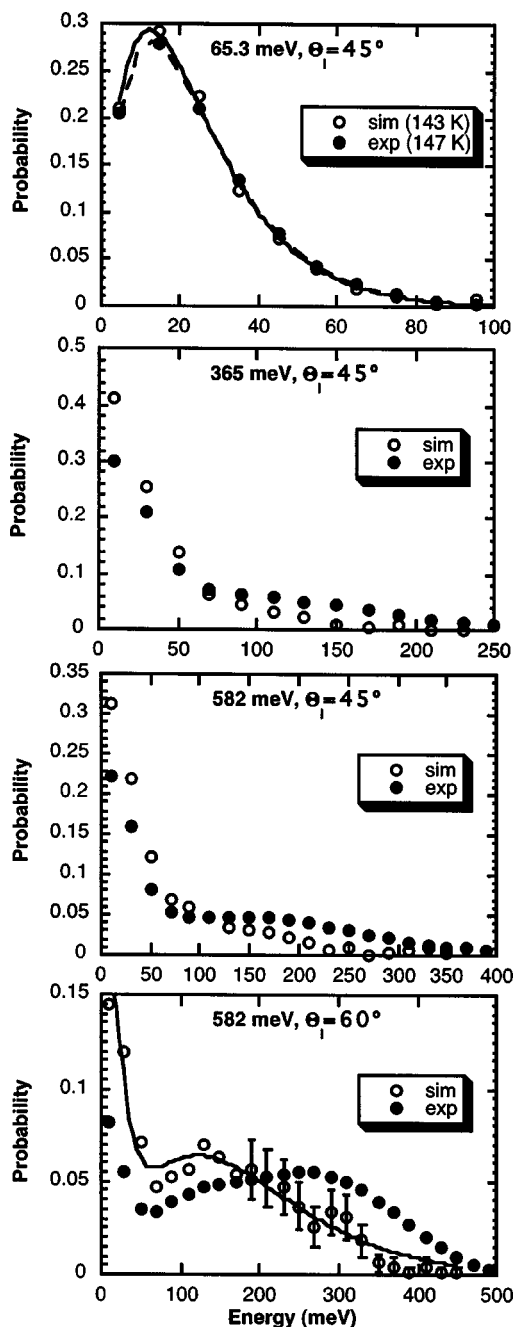

FIG. 8. Plot of the fraction of the initial Ar energy exchanged with the surface as a function of deflection angle $\chi = \Theta_i + \Theta_f$, for the fast component at $T_s = 135$ K and $\Phi_i = 0°$. The inset indicates the incident energy and azimuthal angle. The solid line is from a fit to a binary collision model (see text).

plane formed by the surface perpendicular and the 1-decanethiol axis and the plane of the *trans* backbone. In the model, $\Psi = 90°$. For the comparison between the experiments and simulations, it is important to be aware of the differences between the real and model surfaces. First, the
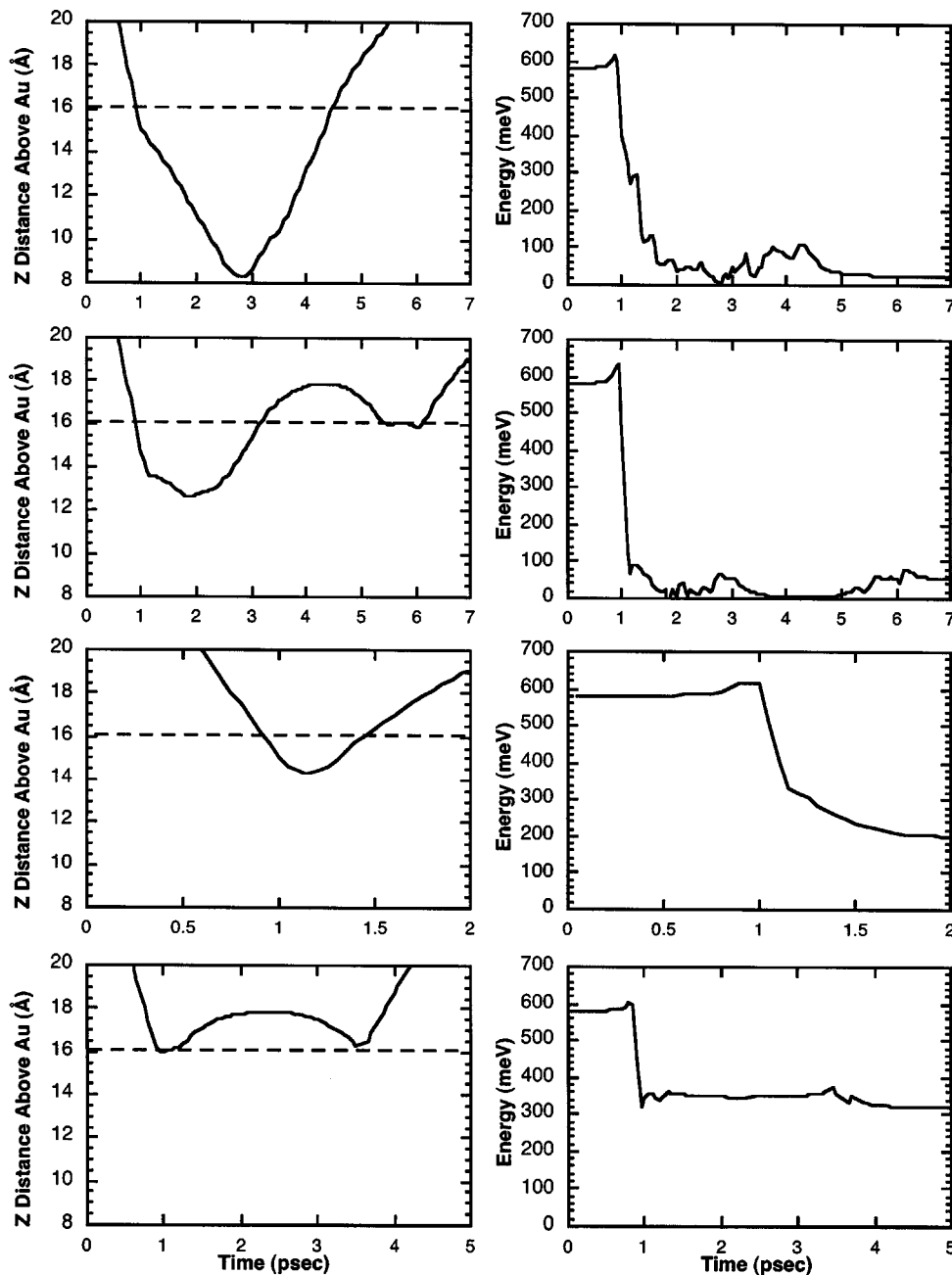
FIG. 10. Examples of some of the trajectory results for $E_i = 582$ meV, $\Theta_i = 45°$, $T_s = 135$ K, and $\Phi_i = 0°$. The left side plots show the z distance from the Au surface as a function of time, with the dashed line the approximate classical turning point for Ar directly above a methyl group of a 1-decanethiol chain at its equilibrium position. Right side plots show the concurrent energy changes.

precise structure of the 1-decanethiol adlayer is still not known.[20] Our experimental diffraction results are consistent with three rotated domains of a $c(4\times2)$ structure; the model would give a strictly $(\sqrt{3}\times\sqrt{3})R30°$ diffraction pattern. Secondly, the molecular beam intersects the crystal in an ellipse with a minor axis of ~1 mm. The size of any surface domain is no more than a few hundred Å^2. Thus the experiment samples many domains, and even within the confines of the simplified model, the tilt direction of the chains could change by 180°, and the azimuthal rotation by ±30°, between these domains. The significance of this will become evident during the discussion.

RESULTS AND DISCUSSION

Incident polar angle and energy dependence

Experiment

Figures 2–4 show examples of time-of-flight (TOF) spectra, after deconvoluting out the cross-correlation pattern. Since the detector uses an electron impact ionizer, the intensity shown is a number density. To fit the data, the model starts with the sum of two velocity distributions:

$$f(v) = a_1 v^3 \exp(-((v-v_0)/\alpha)^2)$$
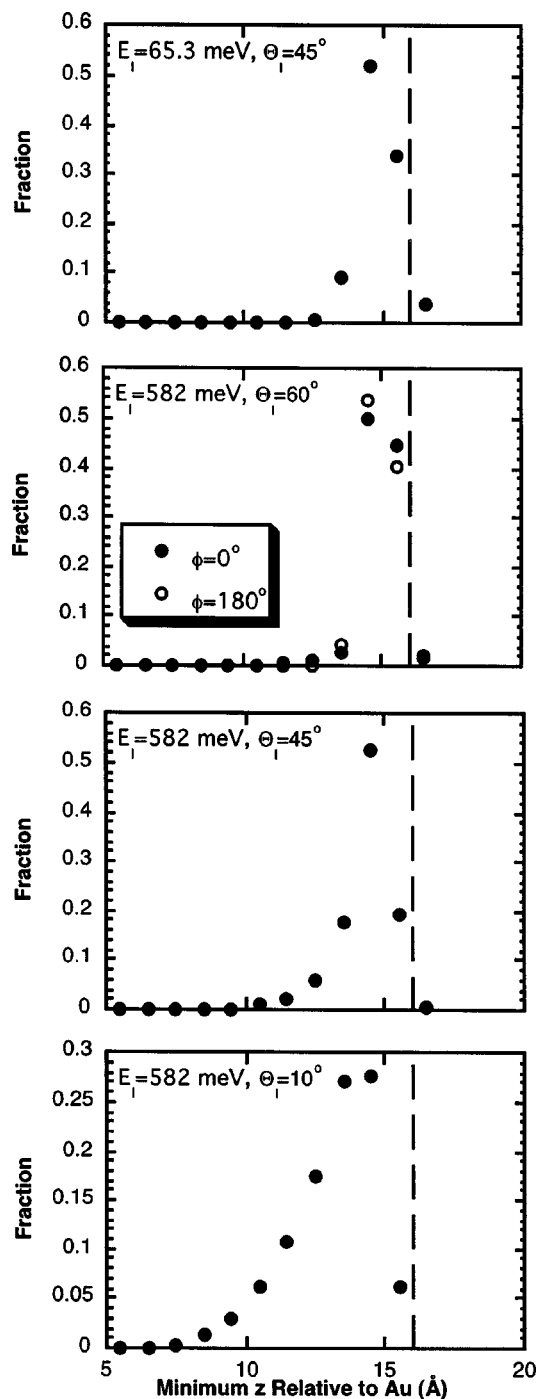$$+ a_2 v^3 \exp(-mv^2/2k_BT_S), \qquad (2)$$

FIG. 11. Probability distributions of the minimum z position that the trajectories reach for some different E_i and Θ_i at $T_s = 135$ K. The vertical dashed lines are at the approximate distance of the hard sphere turning point. Plots are arranged so that the incident perpendicular momentum increases from top to bottom.

FIG. 12. Plots of the final Ar kinetic energies vs Θ_f and Φ_f for $E_i = 582$ meV, $\Theta_i = 60°$, $T_s = 135$ K, and $\Phi_i = 0°$ ($\Phi_F = 180°$ is forward scattering). Plots are for those trajectories that escaped the surface within 20 ps, 896 out of 1500 total, which are principally due to the direct inelastic scattering component.

where a_1, a_2, v_0, and α are fitting parameters and k_B is Boltzmann's constant. The first term is a shifted Maxwell–Boltzmann distribution and represents the inelastically scattered Ar. The second term is a Maxwell–Boltzmann distribution at the surface temperature, expected for trapping-desorption behavior.

This equation must be modified to use as a model for the least-squares fitting routine. The first step involves multiplying this equation by the proper Jacobian to convert to a num-
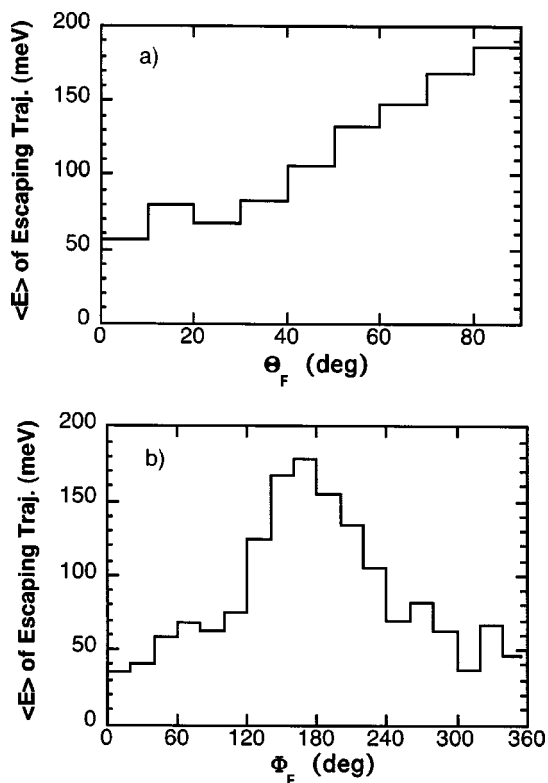
ber density.[21] It must also be corrected for the geometric factors involved in the overlap between the incident beam and the area of the crystal imaged by the well-collimated detector.[22] In practice, the constant a_1 was sometimes weighted with the sum of the first few Hermite polynomials to improve the fit.[23] This was done when Eq. (2) did not fit the data well; the only criterion for whether Hermite polynomials were used and which ones were used was determined by χ^2, the goodness of the fit. For $E_i = 65.3$ meV or any incident energy at $\Theta_i = 10^0$, a_2 was set to 0, since the TOF spectra did not clearly show two distributions (top panel of Fig. 2). In the other cases, the angular intensity distribution is $\cos(\Theta_f)$, which is expected for trapping-desorption. Sometimes, the surface temperature T_s was also varied as a fitting parameter; the results were within 5 K of the measured surface temperature.

Figures 5–7 are summaries of E_f and relative scattered intensities as a function of Θ_f for the different incident angles and energies. In all cases, the measured T_s was 135 K, so that $2k_B T_s = 23.3$ meV. For $E_i = 65.3$ meV, the total final energy is low, and only one peak is used for fitting. At $\Theta_i = 10°$, both the final energy and intensity are indicative of complete trapping-desorption; the energy is ~23 meV, indicating complete thermalization, and the angular intensity variation is distributed as $\cos(\Theta_f)$ over the angular range that can be measured. With more glancing Θ_i, the angular intensity distributions diverge from $\cos(\Theta_f)$ and the final energy increases with increasing Θ_f, showing that at least some of
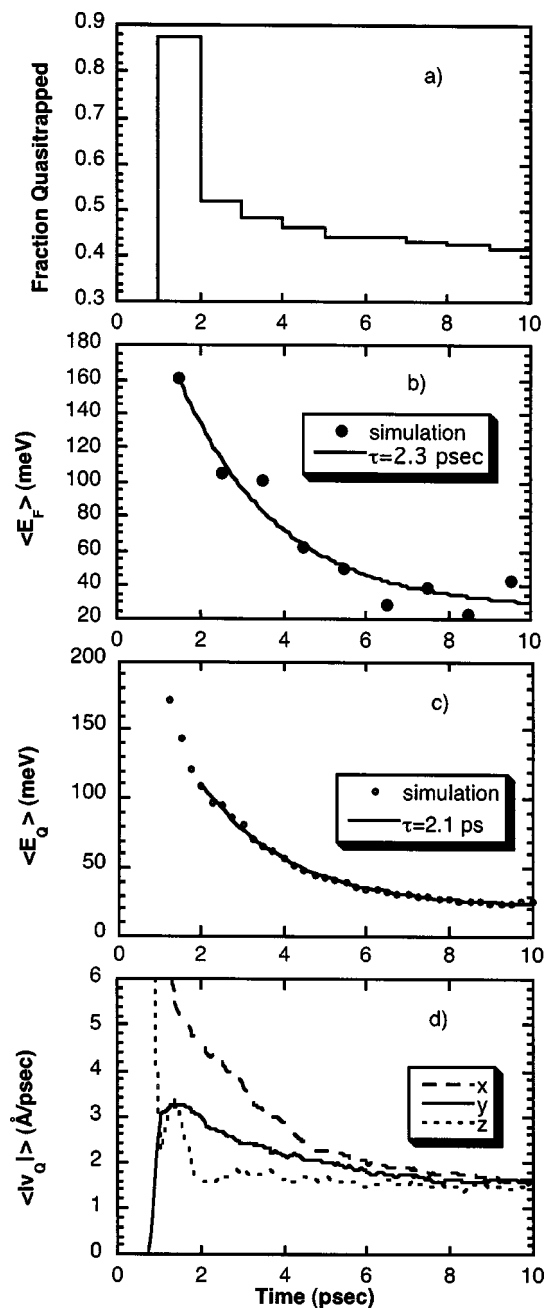
FIG. 13. Panel a shows the fraction of trajectories that are still within 18 Å of the Au after colliding with the surface, plotted as a function of time. $T = 0$ ps is the start of the simulation at ~25 Å. Panel (b) shows the average final kinetic energy for those Ar atoms that have crossed that plane at the indicated time, and panel (c) shows the average kinetic energy of the atoms remaining within 18 Å. The solid lines are from fits to an exponential decay with τ given in the insets. Panel (d) is a plot of the average of the absolute values of the velocity components of the Ar remaining within 18 Å of the Au. Conditions are $E_i = 582$ meV, $\Theta_i = 60°$, $T_s = 135$ K, and $\Phi_i = 0°$.

the scattering is inelastic; the Ar has not had time to equilibrate with the surface before scattering.

At E_i of 365 and 582 meV, there is no angle at which all of the Ar equilibrates with the surface. For $\Theta_i \geq 30°$, there are clearly both direct inelastic and trapping-desorption channels. The intensity of the inelastically scattered component increases with Θ_f, peaking at ~70°, and the relative intensity of the inelastically scattered to the trapping-

desorption components increases as Θ_i increases. The energy of the inelastically scattered component also regularly increases as a function of the deflection angle $\chi = \Theta_i + \Theta_f$.

In light of this last observation, we plotted in Fig. 8 the proportion of direct inelastic Ar–surface energy exchange as a function of the deflection angle for the conditions where there were clearly resolved inelastic and trapping-desorption scattering. The solid line is a fit using Eq. (14) in the discussion of Harris derived from a simple binary collision model[24]

$$\delta E = \frac{2\mu}{(1+\mu)^2}[1+\cos\chi\sqrt{1-\mu^2\sin^2\chi}+\mu\sin^2\chi]E_I,$$

(3)

which gives a value of $\mu = $ (Ar mass)/(Effective surface mass) = 0.62. The model implies that the Ar is scattering from an array of individual scattering centers, which is not unreasonable given that the surface is corrugated and how the distance of the methyl–Ar hard sphere interaction (~3.4 Å) compares to the larger methyl–methyl distance (5 Å). This is obviously not a great model, for instance it is probable that some of the inelastically scattered Ar undergoes multiple collisions. Nevertheless the congruence is worth mentioning.

As a simplified model for this corrugated surface, it is possible to think of the methyl groups as a regular array of spherical scattering centers. Within this approximation, a grazing collision with one of these spheres classically results in less energy being exchanged than for a direct impact. There are more impact parameters that lead to grazing collisions with trajectories that scatter away from the surface at glancing than at near-normal incident angles. For near-normal scattering, multiple collisions lead to a greater energy loss of the scattered Ar when the initial energy is so much greater than $k_B T_S$. This simple observation can qualitatively explain the relative energy of the scattered Ar as shown in Figs. 5–7. It is also known from scattering calculations for rare gas scattering from transition metals[2] and ordered 1-decanethiol that the rate of the momentum accommodation is faster in the normal direction than in the parallel directions. If this is the case for the experiments described in this paper, it would then be expected that the higher energy scattered Ar, which have probably undergone very few collisions and spent only a short time near the surface, would leave near more glancing angles. Normal momentum accommodates faster with the surface than parallel momentum.

The incident angle and energy dependence of the trapping probability is often characterized by $E_i \cos^n(\Theta_i)$.[1] For relatively smooth surfaces, "normal energy" scaling might be expected, where trapping is dependent on the accommodation of the normal component of momentum since the parallel component equilibrates very slowly, particularly with respect to the expected residence time. More corrugated surfaces, which should promote parallel momentum exchange, would exhibit decreasing values of n. If accommodation were equally efficient in both parallel and perpendicular directions, n would be 0, which is called "total energy" scaling.[25] The plots of the intensities of the trapped and scattered intensities, Figs. 5–7, show that the relative intensities depend upon the incident angle; there is not total energy
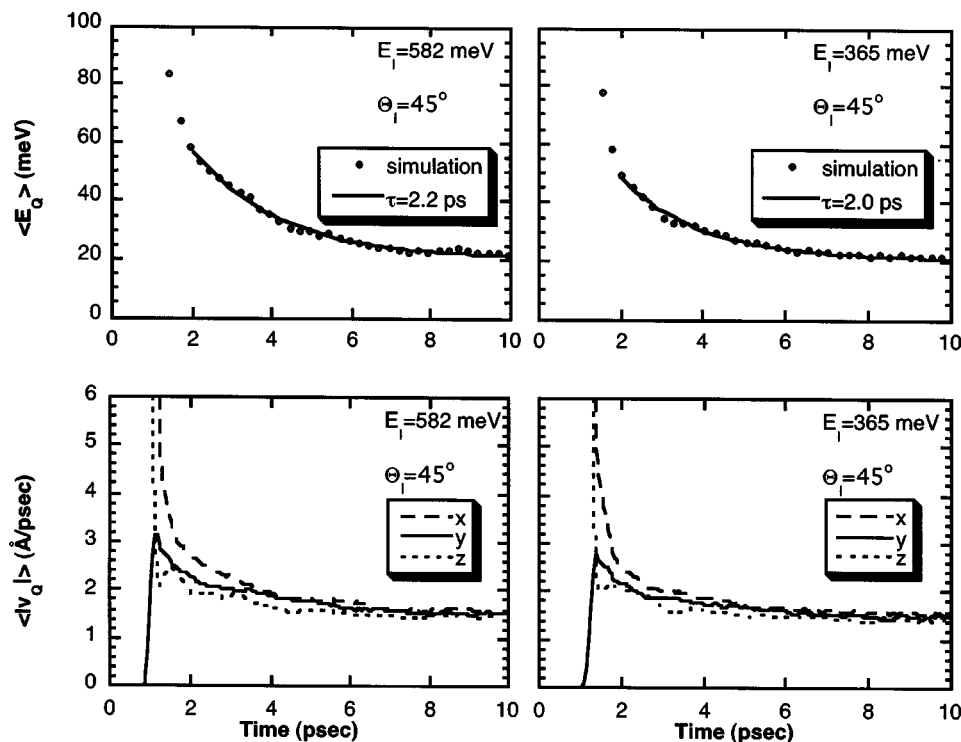
FIG. 14. Plots like those in Figs. 13(c) and 13(d) for different E_i with $\Theta_i = 45°$, $T_s = 135$ K, and $\Phi_i = 0°$.

scaling even though the surface is very corrugated. This is evidence of the slower accommodation of parallel as opposed to perpendicular momentum. To determine the exact value of n, the scattering must be mapped out-of-plane as well as in-plane, something that was not done.

Simulation

As with the papers dealing with Ne scattering,[9,10] the VENUS code was used to assist in understanding the microscopic details of the Ar–surface scattering. The necessary first step is to compare the simulation results for Ar scattering with the experimental results, Fig. 9. It was impossible to run enough trajectories for a direct comparison with the experiment (detector resolution ~1° FWHM) so a wider range of azimuths must be used, as detailed in the captions. Further, some of the trajectories lingered near the surface for many tens of picoseconds, leading to very long calculation times. However, it was found that the simulations could reasonably be truncated at 10–20 ps; Ar leaving the surface after this time had energies consistent with trapping-desorption. Thus, the results shown in Fig. 9 come from calculations that, for the most part, were truncated after 20 ps. Any Ar still near the surface was assumed to be distributed with a Maxwell–Boltzmann velocity distribution, with $\cos(\Theta_f)$ polar and isotropic azimuthal angular intensity variations, and this fraction was added in proportionately. The comparisons are similar, the differences being most pronounced for the higher energy scattered Ar, particularly noticeable for $E_i = 582$ meV and $\Theta_i = 60°$. The agreement is good enough to make qualitative observations about the physics at the surface.

Figure 10 shows the positions and kinetic energies of some of the trajectories at $E_i = 582$ meV, $\Theta_i = 45°$, $T_s = 135$ K and $\Phi_i = 0°$. The z distance is measured from the

static Au surface and the horizontal dashed line is the hard-sphere turning point (average methyl–Au distance of 12.7 Å at 135 K plus an Ar–methyl distance of 3.4 Å). The top trajectory is for an unusual event in that the Ar actually has penetrated below the level of the surrounding methyl groups. It gradually worked its way out from between the chains and escaped with a low energy of 24.5 meV. One general observation is that the Ar energy loss is inversely related to minimum z position for the trajectory, which is a complicated function of where the Ar initially strikes the unit cell. Along with this, it is apparent that the energy loss is directly proportional to the time the Ar is in intimate contact, which is approximately equal to the time the z position is below the dashed line. However, only a few picoseconds are needed to lose much of the initial energy. Two of the trajectories clearly show the loss of most of the initial perpendicular momentum; after the initial collision, they do not have sufficient normal velocity to escape, colliding with the surface a second time. This is especially marked for the bottom trajectory, where the Ar has over 300 meV of kinetic energy after the initial impact, but the momentum is directed almost entirely along the surface, so that atom only escapes after a second impact.

Figure 11 shows the minimum z distance distributions for the simulations. The higher the normal momentum, the closer the normal turning point is to the Au surface. For most of the trajectories, the surface is compressed under the force of the collision. Only in the case of $E_i = 582$ meV and $\Theta_i = 10°$ are there very many trajectories where the Ar actually penetrates below the level of the surrounding methyl groups.

Figure 12 shows the azimuthal and polar angle dependence of the final energy for the Ar that left the surface within 20 ps for $E_i = 582$ meV, $\Phi_i = 0°$, $T_s = 135$ K and $\Theta_i = 60°$. The results are typical for the higher energy scattering
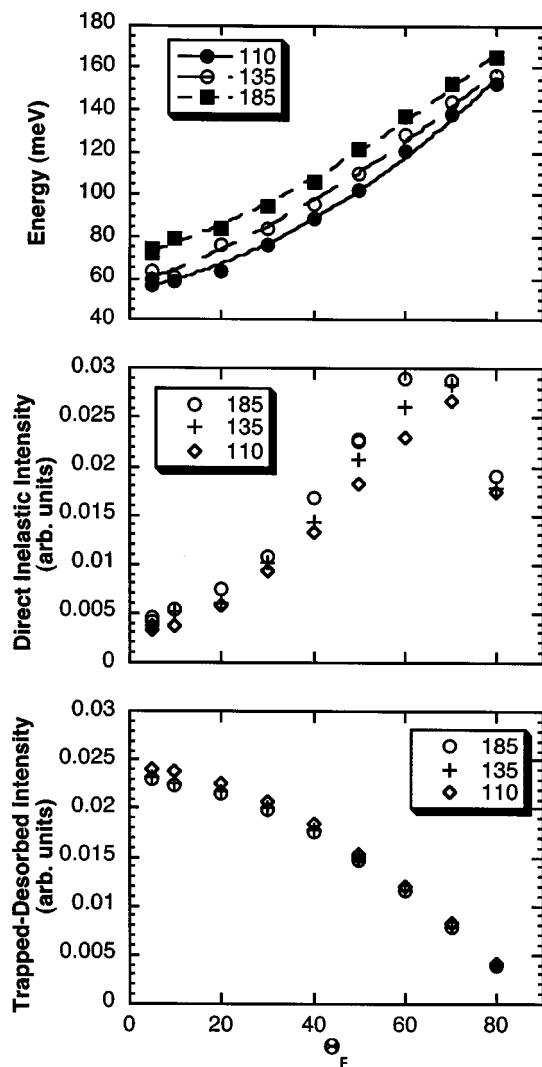
FIG. 15. Plots summarizing the experimental surface temperature dependence for scattering of 365 meV Ar at $\Theta_i = 45°$, and $\Phi_i = 0°$. Top plot shows the average energy of the inelastically scattered component as a function of Θ_f. Lines are from a quadratic fit to the data. The bottom two plots show the relative intensities of the direct inelastic and trapping-desorption components. The latter are from Maxwell–Boltzmann distributions at the surface temperature.

FIG. 16. Example TOF spectra for $\Theta_f = 80°$, $E_i = 625$ meV, and $T_s = 135$ K taken at different Θ_i and two different Φ_i, $0°$, and $30°$. Symbols are the data and lines are the fits.

at glancing angles Θ_i, with the highest scattered energies in the "forward direction," $\Phi_f = 180°$, and at the largest polar angle. The latter two observations are consistent with the fast Ar being due to short interaction times, multiple collisions are needed to totally randomize the parallel momentum, and the perpendicular momentum accommodates faster than the parallel momentum.

Figure 13 summarizes theoretical results for $E_i = 582$ meV, $\Theta_i = 60°$, $\Phi_i = 0°$, and $T_s = 135$ K for trajectories within 18 Å of the static Au surface after first colliding with the 1-decanethiol. 18 Å was chosen since the Ar is still within the tail of the attractive well, but most of the atoms that cross this plane do not return to the surface. The zero of time is the start of the simulation; the Ar first starts strongly interacting with the surface at ~0.6 ps, as shown in Fig. 10. Figure 13(a) shows the fraction of the total trajectories that remain below this plane as a function of time, and Fig. 13(b) shows the average kinetic energy far from the surface of the
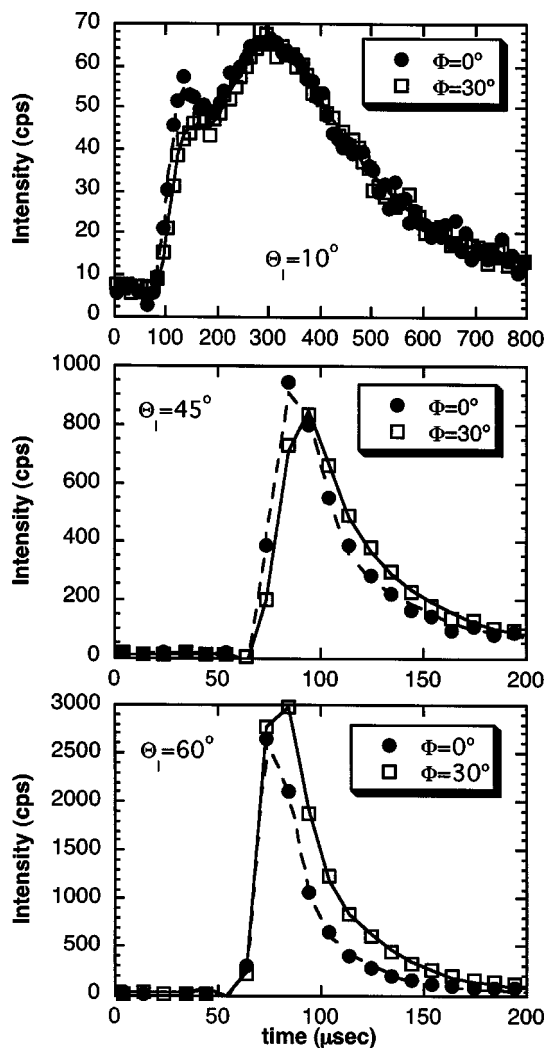
atoms that escaped as a function of the time at which they crossed the 18 Å plane. The vast majority of the atoms that escape with high final energies, which would correspond to the inelastically scattered Ar, has only strongly interacted with the surface for ~1 ps. After this time, the number escaping per unit time is very small, and the average final kinetic energy approaches $2k_B T_s$. Figure 13(c) shows the average kinetic energy of the Ar trajectories still below the 18 Å plane, which will be referred to as quasi-trapped. In both Figs. 13(b) and 13(c), the tail of the average energy plots have been fit to an exponential decay, giving a time constant τ of ~2 ps. Figure 13(d) shows the average of the absolute values of the quasi-trapped Ar velocity components as a function of time. The trajectories start in the $x-z$ plane, so the y velocity is 0 Å/ps until the surface collision occurs. From this comparison, it can be seen that the normal component nearly reaches steady state within ~2 ps, while the x and y components take about 8 ps. The conclusion is that complete accommodation to the surface is very rapid, with the normal direction happening in <2 ps, which generally confines the Ar to a trajectory parallel to the surface, where it
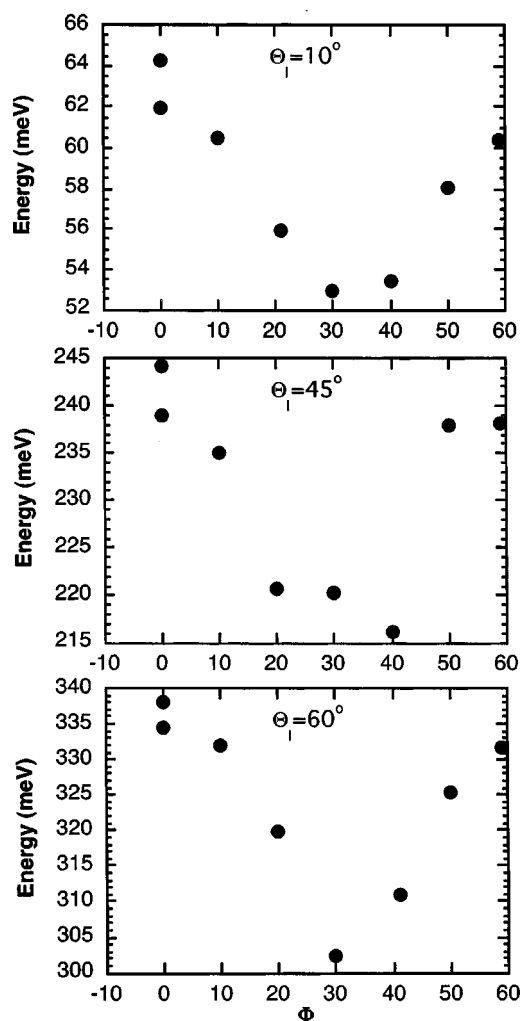
FIG. 17. Experimentally measured total average kinetic energy as a function of Φ_i at three different Θ_i. For all of the results, $\Theta_f=80°$, $E_i=625$ meV, and $T_s=135$ K.

FIG. 18. Comparison of the simulations for $E_i=582$ meV, $\Theta_i=60°$, and $T_s=135$ K for incident azimuths of $0°$ and $180°$. In both cases there were 1500 trajectories, and all are included. The simulation was truncated after 20 ps, and the trajectories that had not concluded were considered to be thermalized and were added accordingly (see text).

loses much of its remaining momentum over a somewhat longer time frame. The atoms that do escape quickly have lost more of their initial z velocity than in-plane velocity, so higher final energies occur at more glancing final angles. The same general behavior, the more rapid accommodation of perpendicular than parallel momentum, is postulated for smooth metal surfaces. In the case of the metals, the parallel momentum accommodation takes an order of magnitude longer time as compared to the 1-decanethiol surface.[2]

Figure 14 shows the results for two additional incident conditions. At $E_i=582$ meV and $\Theta_i=45°$, where the initial normal velocity is higher than at $\Theta_i=60°$, the z velocity takes comparatively longer, and the parallel velocity comparatively shorter, to reach a steady state. The z-velocity accommodation still occurs faster than for the parallel velocity. The same observations hold at $E_i=365$ meV and $\Theta_i=45°$. In both cases, the average kinetic energy decay constant is still ~2 ps, which implies that the total momentum accommodates at the same rate for all of these conditions.

Temperature dependence

Experiments comparing the scattering of Ar from surfaces at different T_s were also performed. A summary for the
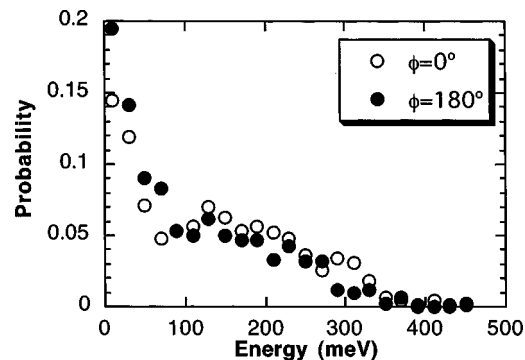
conditions $E_i=365$ meV, $\Theta_i=45°$, and $\Phi_i=0°$ is shown in Fig. 15. For the trapping-desorption component, the intensity was fit to a cosine angular intensity profile at the surface temperature. The top panel shows the average kinetic energy of the inelastically scattered component as a function of Θ_f. Qualitatively, the decrease in energy transferred with the increase in T_s is what would be expected from a simple classical scattering model.[24] For the range of temperatures shown here, the proportionality constant is $\sim2.7k_B\Delta T_s$. The lower panels show the relative intensities of the direct inelastic and trapping-desorption components. The inelastic scattering intensity increases slightly with T_s over the temperature range. The reason for the apparently smaller drop in the trapping-desorption intensity is that this component is scattered over a Φ_f of 360°, rather than just being forward scattered, as is the case for the direct inelastic component.

Incident azimuthal angle

As mentioned in the introduction, we also investigated the dependence of the Ar scattering on Φ_i. Any effect should be best observable at glancing final angles since these are the scattered atoms that have had the fewest collisions with the surface; the motion of the Ar does not randomize with shorter interaction times. It was also found that higher incident energies gave the clearest results. Figure 16 shows the comparison of TOF spectra at different Θ_i with Φ_i separated by 30° relative to the Au$\langle1\bar{1}0\rangle$ direction, defined as $\Phi_i=0°$, with $E_i=625$ meV and $\Theta_f=80°$ at $T_s=135$ K. For $\Theta_i=10°$, where much of the Ar undergoes trapping-desorption, there is a distinctly larger high-energy peak at $\Phi_i=0°$ as compared to the results at $\Phi_i=30°$. For Θ_i equal to 45° and 60°, where much more is inelastically scattered, the difference is a shift in the TOF feature to shorter times at $\Phi_i=0°$ as compared to the results at $\Phi_i=30°$. In all cases, the average energy is higher at $\Phi_i=0°$. Figure 17 summarizes the average total kinetic energy of the scattered atoms as a function of the azimuthal direction. The energy vs azimuthal angle plots at different incident polar angles have a minimum at $\Phi_i=30°$ and approximately the same values at $\Phi_i=0°$ and 60°. We also compared $\Phi_i=-30°$ and 30°, and the intensities were identical. Φ from $-30°$ to 60° was the

extent of the available crystal adjustment, but within these limits, the results suggest a sixfold symmetry.

Though the model is a simplified version of reality, it has features that have a good experimental basis. One of these features, which also breaks rotational symmetry about the surface normal, is the chain tilt. Simulations were performed to investigate how the angle of incidence relative to the chain tilt could affect the results. Though it would have been time-consuming to run simulations at all possible chain positions consistent with the model, some idea can be obtained by investigating two opposing directions at $E_i = 582$ meV, $\Theta_i = 60°$ and $T_s = 135$ K: $\Phi_i = 0°$ (approximately against the chain tilt) and $\Phi_i = 180°$ (approximately with the chain tilt). These simulations are not meant to be used as a direct comparison with the experimental results, but only to demonstrate that the response of the self-assembled monolayer surface to the impinging Ar is highly dependent on *both* azimuthal and polar angles. The resulting energy distributions for 1500 trajectories are shown in Fig. 18. As before, any trajectories that had not concluded after 20 ps (604 for $\Phi_i = 0°$ and 770 for $\Phi_i = 180°$) were added in as a Maxwell–Boltzmann energy distribution at the $T_s = 135$ K. The one clear and statistically significant feature is that more Ar is trapped when $\Phi_i = 180°$, as seen by the difference in the probabilities at low energy, and by the number of trajectories that had not left the surface after 20 ps, 604 versus 770, as mentioned above.

Figure 19 summarizes the trajectory information near the surface. Figure 19(a) shows the relative fraction and Fig. 19(b) the average final kinetic energy of the Ar that escaped plotted as a function of the time at which they crossed the plane 18 Å above the static Au surface. The biggest difference is the number that escaped within the first 2 ps, there are much more at $\Phi_i = 0°$ than at 180°. These are the atoms that transfer the least energy to the surface. The result is that the average kinetic energy is higher at $\Phi_i = 0°$. This behavior was also observed for Ne scattering.[9] Figure 19(c) shows a comparison of the average kinetic energy of the quasi-trapped atoms as a function of time. At short times, the average E_Q is consistently higher at $\Phi_i = 180°$ than 0°. In both cases, the results can be fitted to an exponential decay with an ~2 ps time constant. Figure 19(d) shows the average value of the absolute value of the x component of velocity. It appears that at $\Phi_i = 180°$ the normal component of the momentum is more quickly accommodated, but the momentum in the scattering plane parallel to the surface is *more slowly* accommodated; the Ar has insufficient velocity to escape the surface but is still moving fairly rapidly along the surface.

To get some idea of the mechanism, simulations were done with the surface initially static, since at 135 K the thermal motion of the surface makes it difficult to extract the collision-induced motion. Compared with $\Phi_i = 180°$, the trajectories at $\Phi_i = 0°$ resulted in the excitation of higher energy modes immediately after collision. At $\Phi_i = 180°$, the modes consist principally of collective wagging of the chains. At $\Phi_i = 0°$, in addition to the collective wagging, there are more CCC torsions and CCC bending of the chains.
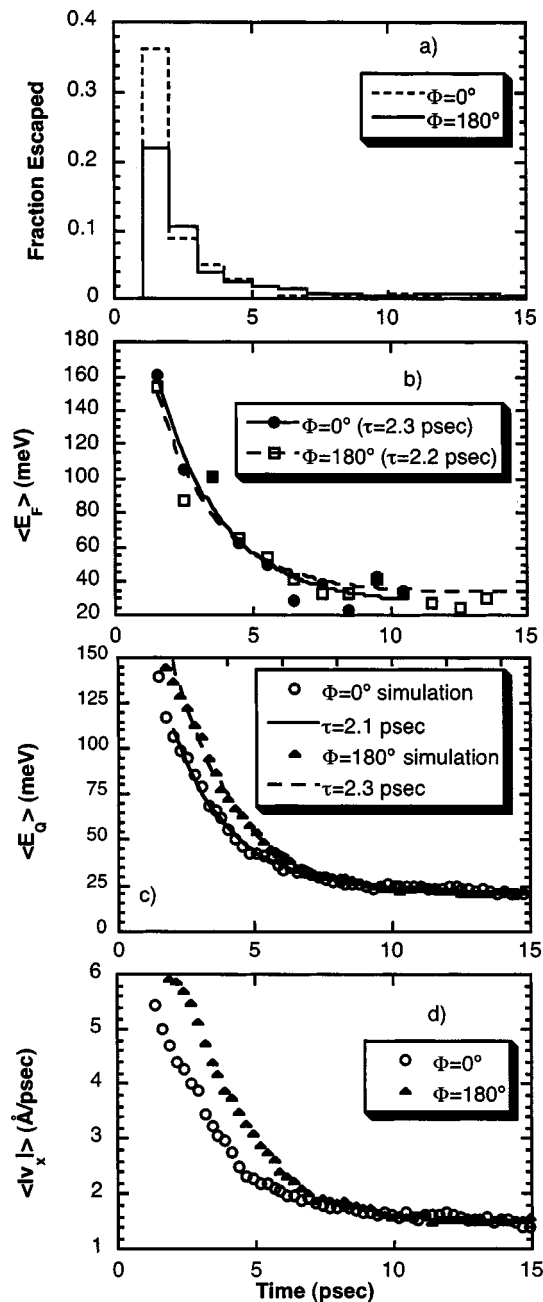

FIG. 19. Comparison of the simulation results for the two different Φ_i, for $E_i = 582$ meV, $\Theta_i = 60°$, and $T_s = 135$ K. Trajectories at all angles are included, with a total of 1500 for each azimuth. Panel (a) shows the fraction of trajectories that escaped plotted vs the time at which they crossed a plane 18 Å above the Au. Time=0 is the start of the simulation at ~25 Å. Panel (b) shows the average final kinetic energy for those Ar atoms that have crossed that plane at the indicated time, and panel (c) shows the average kinetic energy of the atoms remaining within 18 Å. The lines are from fits to an exponential decay with τ given in the inset. Panel (d) is a plot of the average of the absolute values of the x component of the velocity of the Ar remaining within 18 Å of the Au substrate.

CONCLUSIONS

In this paper, we have both experimentally and theoretically investigated the scattering of Ar from an ordered standing phase of 1-decanethiol adsorbed on a Au(111) surface. The polar and azimuthal angular intensity and energy distributions of the scattered Ar as a function of incident conditions were measured. These were compared with the results

of classical trajectory calculations. A reasonable agreement allows for the inference of the physics at the surface that cannot be presently measured.

For all of the E_i used (65–600 meV), a significant amount of the incident Ar undergoes trapping-desorption, leaving the surface with a cosine angular intensity profile and with an energy thermalized with the surface. The intensity of this component relative to the direct inelastic increases with decreasing E_i and decreasing Θ_i. Though the surface is very corrugated, the trapping probability does not follow "total energy" scaling. Instead, the energy and intensity of the scattered Ar increases towards glancing angles, which suggests that the parallel momentum accommodates to the surface slower than the perpendicular momentum.

The simulations show that most of the Ar that directly scatters interacts with the surface for <2 ps. It is scattered in the forward direction, particularly for the higher incident energies and angles. In this time period, the Ar does not undergo enough collisions to totally randomize the motion. Further, the normal momentum is accommodated faster than parallel momentum. These observations are in agreement with the experimental results.

Since the normal momentum is accommodated faster than parallel momentum, it is possible for Ar to be trapped near the surface, but still be translating rapidly along the surface. Some of these trajectories are deflected into the gas phase by the collisions with the corrugated surface, but the relaxation time for the exponential decay of this energy is only ~2 ps. Thus, atoms that are not promptly scattered are quickly thermalized with the 1-decanethiol.

Experimentally, there is evidence of a sixfold symmetric azimuthal angle dependence in the final energy for the direct inelastic scattering. One possible reason for this dependence is that the 1-decanethiol chains are tilted by ~34° to the surface normal, which breaks the rotational symmetry. The simulation shows that Ar colliding with the surface at different Φ_i changes the motions of the chains that are primarily excited, leading to different degrees of energy accommodation. Rare-gas scattering is often used to determine surface structure by measuring the scattered intensity as a function of incident angles. In the case of the 1-decanethiol monolayer, the structural information is contained in the energy exchanged between the atom and surface as a function of angle.

ACKNOWLEDGMENTS

[1] B. Berenbak, S. Zboray, B. Riedmuller, D. C. Papageorgopoulos, S. Stolte, and A. W. Kleyn, Phys. Chem. Chem. Phys. **4**, 68 (2002); M. D. Ellison, C. M. Matthews, and R. N. Zare, J. Chem. Phys. **112**, 1975 (2000); C. T. Rettner, D. S. Bethune, and D. J. Auerbach, *ibid.* **91**, 1942 (1989); C. B. Mullins, C. T. Rettner, D. J. Auerbach, and W. H. Weinberg, Chem. Phys. Lett. **163**, 111 (1989); J. E. Hurst, Jr., L. Wharton, K. C. Janda, and D. J. Auerbach, J. Chem. Phys. **83**, 1376 (1985); **78**, 1559 (1983).

[2] M. Head-Gordon, J. C. Tully, C. T. Rettner, C. B. Mullins, and D. J. Auerbach, J. Chem. Phys. **94**, 1516 (1991).

[3] R. J. W. E. Lahaye, A. W. Kleyn, S. Stolte, and S. Holloway, Surf. Sci. **338**, 169 (1995); R. J. W. E. Lahaye, S. Stolte, A. W. Kleyn, R. J. Smith, and S. Holloway, *ibid.* **307–309**, 187 (1994); R. J. Smith, A. Kara, and S. Holloway, *ibid.* **281**, 296 (1993).

[4] E. P. Wenass, J. Chem. Phys. **54**, 376 (1971).

[5] C. T. Rettner, E. K. Schweizer, and C. B. Mullins, J. Chem. Phys. **90**, 3800 (1989).

[6] D. Chase, M. Manning, J. A. Morgan, G. M. Nathanson, and R. B. Gerber, J. Chem. Phys. **113**, 9279 (2000); L. Tribe, M. Manning, J. A. Morgan, M. D. Stephens, W. R. Ronk, E. Treptow, G. M. Nathanson, and J. L. Skinner, J. Phys. Chem. B **102**, 206 (1998); M. E. King, K. M. Fiehrer, G. M. Nathanson, and T. K. Minton, J. Phys. Chem. A **101**, 6556 (1997); G. M. Nathanson, P. Davidovits, D. R. Worsnop, and C. E. Kolb, J. Phys. Chem. **100**, 13007 (1996); M. E. King, M. E. Saecker, and G. M. Nathanson, *ibid.* **101**, 2539 (1994); N. Lipkin, R. B. Gerber, N. Moiseyev, and G. M. Nathanson, *ibid.* **100**, 8408 (1994).

[7] P. U. Andersson, M. B. Nagard, K. Bolton, M. Svanberg, and J. B. C. Pettersson, J. Phys. Chem. A **104**, 2681 (2000); K. Bolton, M. Svanberg, and J. B. C. Pettersson, J. Chem. Phys. **110**, 5380 (1999); K. Bolton and J. B. C. Pettersson, Chem. Phys. Lett. **312**, 71 (1999).

[8] S. F. Shuler, G. M. Davis, and J. R. Morris, J. Chem. Phys. **116**, 9147 (2002).

[9] N. Isa, K. D. Gibson, T. Yan, W. L. Hase, and S. J. Sibener, J. Chem. Phys. (to be published).

[10] T. Yan, W. L. Hase, N. Isa, K. D. Gibson, and S. J. Sibener, J. Phys. Chem. A (to be published).

[11] S. B. M. Bosio and W. L. Hase, J. Chem. Phys. **107**, 9677 (1997).

[12] T. Yan, W. L. Hase, and J. R. Barker, Chem. Phys. Lett. **329**, 84 (2000).

[13] T. Yan and W. L. Hase, Phys. Chem. Chem. Phys. **2**, 901 (2000).

[14] T. Yan and W. L. Hase, J. Phys. Chem. A **105**, 2617 (2001).

[15] N. Isa, K. D. Gibson, and S. J. Sibener (unpublished).

[16] J. I. Colonell, K. D. Gibson, and S. J. Sibener, J. Chem. Phys. **103**, 6677 (1995).

[17] W. L. Hase, R. J. Duchovic, X. Hu *et al.*, QCPE **16**, 671 (1996).

[18] J. M. Haile, *Molecular Dynamics Simulation: Elementary Methods* (Wiley, New York, 1992).

[19] G. Liuti, F. Pirani, U. Buck, and B. Schmidt, Chem. Phys. **126**, 1 (1988).

[20] L. Zhang, W. A. Goddard III, and S. Jiang, J. Chem. Phys. **117**, 7342 (2002); Y. W. Yang and L. J. Fan, Langmuir **18**, 1157 (2002); F. Schreiber, Prog. Surf. Sci. **65**, 151 (2000); P. N. Floriano, O. Schlieben, E. E. Doomes, I. Klein, J. Janssen, J. Hormes, E. D. Poliakoff, and R. L. McCarley, Chem. Phys. Lett. **327**, 447 (2000); G. J. Kluth, C. Carraro, and R. Maboudian, Phys. Rev. B **59**, R10449 (1999); P. Fenter, Thin Films **24**, 111 (1998); P. Fenter, F. Schreiber, L. Berman, G. Scoles, P. Eisenberger, and M. J. Bedzyk, Surf. Sci. **412/413**, 213 (1998); N. Camillone III, T. Y. B. Leung, and G. Scoles, *ibid.* **373**, 333 (1997).

[21] D. J. Auerbach, in *Atomic and Molecular Beam Methods*, edited by G. Scoles (Oxford University Press, New York, 1988), Vol. 1, p. 362.

[22] G. Comsa and R. David, Surf. Sci. Rep. **5**, 145 (1985).

[23] H. C. W. Beijerinck, G. H. Kaashoek, J. P. M. Beijers, and M. J. Verheijen, Physica B & C **121B+C**, 425 (1983).

[24] J. Harris, in *Dynamics of Gas–Surface Interactions*, edited by C. T. Rettner and M. N. R. Ashfold (The Royal Society of Chemistry, Cambridge, 1991).

[25] W. H. Weinberg, in *Dynamics of Gas–Surface Interaction*, edited by C. T. Rettner and M. N. R. Ashfeld (The Royal Society of Chemistry, Cambridge, 1991).